Received: 27 March 2021 | Revised: 4 January 2023 | Accepted: 19 January 2023

DOI: 10.1002/zamm.202100112

ORIGINAL PAPER

Accessing the thermodynamics of Walter-B fluid with magnetic dipole effect past a curved stretching surface

Noor Saeed Khan[1] | **Abid Hussanan**[1] | **Wiyada Kumam**[2] | **Poom Kumam**[3,4,5] | **Panawan Suttiarporn**[6]

[1]Department of Mathematics, Division of Science and Technology, University of Education, Lahore, Pakistan

[2]Program in Applied Statistics, Department of Mathematics and Computer Science, Faculty of Science and Technology, Rajamangala University of Technology Thanyaburi (RMUTT), Pathum Thani, Thailand

[3]KMUTTFixed Point Research Laboratory, Fixed Point Laboratory, Department of Mathematics, Faculty of Science, King Mongkut's University of Technology Thonburi (KMUTT), Bangkok, Thailand

[4]Center of Excellence in Theoretical and Computational Science (TaCS-CoE), Science Laboratory Building, Faculty of Science, King Mongkut's University of Technology Thonburi (KMUTT), Bangkok, Thailand

[5]Department of Medical Research, China Medical University Hospital, China Medical University, Taichung, Taiwan

[6]Faculty of Science, Energy and Environment, King Mongkut's University of Technology North Bangkok, Rayong Campus, Rayong, Thailand

Correspondence
Poom Kumam, KMUTTFixed Point Research Laboratory, Fixed Point Laboratory, Department of Mathematics, Faculty of Science, King Mongkut's University of Technology Thonburi (KMUTT), Bangkok 10140, Thailand.
Email: poom.kum@kmutt.ac.th

Funding information
Center of Excellence in Theoretical and Computational Science, Grant/Award Number: TaCS-CoE; KMUTT; National Science, Research and Innovation Fund (NSRF); King Mongkut's University of Technology North Bangkok, Grant/Award Number: KMUTNB-FF-66-61; HEC; SRGP, Grant/Award Number: 10534

The effects of magnetic dipole, porosity and heat transfer on the flow of ferromagnetic Walter-B fluid past a curved stretching sheet is investigated with the gyrotactic microorganisms motion and cubic autocatalysis chemical reactions. The momentum, energy, homogeneous–heterogeneous chemical reactions and gyrotactic microorganisms motion equations, form the problem's governing equations, which are transformed into non-linear ordinary differential equations via similarity transformations and are solved using an efficient and strong technique namely homotopy analysis method. The effects of the parameters under consideration on dimensionless velocity, temperature, homogeneous–heterogeneous chemical reaction, and motile microorganisms are graphically depicted and discussed in detail. Velocity decreases with the increasing values of curvature parameter while the magnetic dipole effect and Curie temperature parameter increase the heat transfer. The homogeneous chemical reaction and the motile density of microorganisms are enhanced with the rising values of elasticity and ferromagnetic interaction parameters.

1 | INTRODUCTION

Magnetohydrodynamics (MHD) is applied in various manufacturing fields like polymer and petroleum industry. It is also used in gem developing, metal casting, electric heater and for cooling purposes like in cooling the dividers of interior atomic reactor. MHD flows have a vital role in bio designing, nuclear fuels, cancer tumor treatment, blood pump machine, micro-electro-mechanical systems, avionics, robotics, lasers, aerodynamics, computer peripherals, crystalline, amorphos alloys, MHD generators, flow meters, accelerator pumps, electrochemical, electrical, and mechanical gadgets. Ferrofluids are magnetized fluids that are the suspension of ferromagnetics nanoscale particles in liquid bearer like oragnic solvent or water. Andersson and Vanes [1] investigated the effect of dipole on ferrofluid. Ali et al. [2] used the finite element method to find the solution of a water–ethylene glycol base fluid with single-wall and multi-wall carbon nanotube nanoparticles micropolar ferromagnetic fluid. Alfannakh [3] examined the combined effects of slip, thermophoretic dust particle diffusion and magnetic dipole on the flow of water base fluid with single-wall and multi-wall carbon nanotube nanoparticles towards a stretchable sheet. Waqas et al. [4] studied the biconvection due to gyrotactic microorganisms in Jeffery nanofluid with magnetic dipole past a stretching sheet by numerically solving the problem equations through a bvp4c solver in Matlab. Bashir et al. [5] elaborated the heat and mass transfer in Oldroyd-B fluid with magnetic dipole, gyrotactic microorganisms and chemical reaction under Cattaneo–Christov heat flux theory. Souayeh et al. [6] used the Runge–Kutta technique with shooting method for the solution of mathematical model of Maxwell nanofluid flow with magnetic dipole, non-uniform heat source/sink and chemical reaction. Sajjad et al. [7] interpreted the effects of magnetic dipole, viscous and Ohmic dissipations on a radiative Eyring–Powell fluid flow past a stretching sheet. Gowda et al. [8] explored the Stefan blowing flow of ferrofluid past a flat stretching sheet using Buongiorno model and convective boundary conditions. Kumar [9] considered the magnetic dipole on the water base nanofluid past a stretching sheet who showed that skin friction and Nusselt number are reduced by increasing the second-grade fluid parameter. Related studies can be seen in the references [10–18].

Heat transfer has important applications in industries which is directly related to production cost. Thermal conductivity is affected by the temperaure differences on high scale. Nowadays reserachers have paid special attention in investigating the heat transfer. Reddy et al. [19] worked on the variable thermal conductivity and magnetic dipole effect over a Blasius-Rayleigh–Stokes flow. Gowda et al. [20] studied the second-grade fluid past a curved stretching sheet in which the Newtonian heating parameter increases the heat transfer coefficient. Babu et al. [21] scrutinized the physical aspects of flow and heat transport in non-Newtonian (Carreau–Yasuda) fluid through an upper paraboloid surface of revolution by considering the non-linear radiation, magnetic field, and heat generation. Sheikholeslami et al. [22] discussed the helical tape with various width ratio for augmenting the flow blockage which has great applications in engineering fields and heat exchangers. Tripathi et al. [23] analyzed the peristaltic pumping of water-based titanium dioxide and silver couple stress hybrid nanofluids with the effects of magnetic field, Joule heating and buoyancy. Sheikholeslami et al. [24] presented the empirical and numerical analysis of thermal performance in flat plate solar collectors in which the productivity of photovoltaic modules are reduced by enhancing the temperature. Reddy and Kumar [25] worked on the Cattaneo-Christov heat flux theory for carbon nanotubes embedded in micropolar fluid past a melting surface. Sheikholeslami et al. [26] investigated the effect of aluminum oxide suspended in water for turbulent flow using multiple twisted taps in a solar flat plate by considering the entropy and thermal behavior. Reddy et al. [27] addressed the Cattaneo-Christov heat flux theory for a Blasius–Rayleigh–Stokes flow by applying the Runge-Kutta-Fehlberg 45th-order method. Sheikholeslami and Farshad [28] applied the homogeneous model for hybrid nanomaterial by choosing the six-lobed tube equipped with combined turbulators which provided better cooling performance and lower exergy loss. Shehzad et al. [29] considered the MHD incompressible bioconvective flow of Maxwell fluid in rotating system by adopting the Cattaneo–Christov heat and mass flux model. Further studies about heat transfer and other aspects associated to fluids can be seen in the references [30–44].

Curved surfaces have important applications in liquid crystals in condensation processes, polymer sector, roll-paper manufacturing, designing cycles, glass fibers, annealing copper wires, filaments and so on. Ashraf and Haq [45] worked on the formulation and solution of carreau fluid over a curved stretching surface with homogeneous–heterogeneous chemical reactions and viscous dissipation in which they proved that the Weissenberg number enhances the flow and heat transfer. Jawad et al. [46] focused on the two dimensional MHD boundary layer flow of nanoliquid past a curved stretching sheet with heat source/sink using homotopy analysis method for the solution of the problem. Abbas et al. [47] analyzed a viscous fluid flow with prescribed surface temperature and prescribed heat flux in the presence of constant applied magnetic field past a curved stretching sheet. Hayat et al. [48] addressed the flow of viscous fluid with Cattaneo–Christov double diffusive through a Darcy–Forchheimer porous medium generated by unsteady curved stretching surface. Rabeeah et al. [49] discussed the incompressible steady Williamson fluid flow with thermal radiation over the curved surface in which the curvature parameter reduces the velocity and temperature profiles. Abbas et al. [50] developed a mathematical model for the two-dimensional curvilinear boundary layer flow and heat transfer in an electrically conducting water base nanofluid with Cu and Ag nanoparticles. Muhammad et al. [51] computed the numerical solution through NDSolve technique of Darcy–Forchheimer viscous fluid flow with Cattaneo–Christov heat and mass flux. Waqas et al. [52] presented the hydromagnetic transport of hybrid nanoliquids past a curved surface with thermal radiation, heat source/sink and Lorentz forces effects. Some relevant studies can be found in the references [53–68].

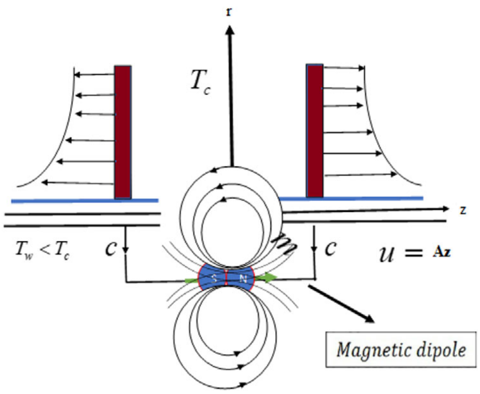

FIGURE 1 Physical sketch of the problem.

The present problem is modeled for the curved surface under the effect of magnetic dipole in the presence of gyrotactic microorganisms and cubic autocatalysis chemical reactions in Walter-B fluid which is solved through the analytical method namely homotopy analysis method [69–81].

2 | FORMULATIONS

Two dimensional incompressible hydrodynamic ferromagnetic Walter-B fluid past a curved stretched surface subject to homogeneous–heterogeneous reactions is analyzed. Gyrotactic microorganisms motion and the effect of magnetic dipole with viscous dissipation are also considered. The z and r are used for curvilinear coordinates. The stretching surface is curled in a radius circle R'. Based on the linear velocity u, the sheet is stretched in $z-$direction while $r-$direction is transversed to the $z-$direction. The strength of the magnetic field is perpendicular to the flow direction (please see Figure 1). The surface is immersed in a porous medium. As the Reynolds number (due to magnetic field) is smaller, the electrical field and the induced magnetic field are ignored. Convective heat transfer conditions are applied. A simple homogeneous-heterogeneous reaction model is assumed to exist as proposed by Merkin [44] in the following form

$$E_1 + 2E_2 \to 3E_2, \quad rate = k_1 C_1 C_2^2, \tag{1}$$

while there is a single isothermal, first-order reaction on the catalytic surface which is

$$E_1 + 2E_2 \to 3E_2, \quad rate = k_2 C_1, \tag{2}$$

where C_1 and C_2 are the concentrations of chemical reactants E_1 and E_2, respectively. k_1 and k_2 are the rate constants. Both reaction processes are assumed to be isothermal in nature.

The boundary layer equations that govern the flow can be written in dimensional form under the above assumptions as [22, 74]

$$\frac{\partial\{(r+R')\upsilon\}}{\partial r} + R'\frac{\partial u}{\partial z} = 0, \tag{3}$$

$$\frac{u^2}{r+R'} = \frac{1}{\rho}\frac{\partial p}{\partial r}, \tag{4}$$

$$\begin{aligned}
\rho\left(\upsilon\frac{\partial u}{\partial r} + \frac{R'u}{r+R'}\frac{\partial u}{\partial z} + \frac{u\upsilon}{r+R'}\right) &= u_e\frac{dU_e}{dz}\frac{R'}{r+R'}\frac{\partial p}{\partial z} + \mu\left(\frac{\partial^2 u}{\partial r^2} - \frac{u}{(r+R')^2} + \frac{1}{r+R'}\frac{\partial u}{\partial r}\right)\\
&- k_0\left(\frac{2u}{(r+R')^2}\frac{\partial^3 u}{\partial z\partial r^2} + \frac{2\upsilon}{r+R'}\frac{\partial^3 u}{\partial r^3} + \frac{R'}{r+R'}\frac{\partial u}{\partial z}\frac{\partial^2 u}{\partial r^2} - \frac{2R'}{(r+R')^2}\frac{\partial u}{\partial r}\frac{\partial^2 u}{\partial r\partial z}\right) - \frac{\nu}{k_o^*}u\\
&- Fru^2 + \mu_o m\frac{\partial H}{\partial z},
\end{aligned} \tag{5}$$

$$(\rho C_p)\left(\frac{R'u}{r+R'}\frac{\partial T}{\partial z}+v\frac{\partial T}{\partial r}\right)=\frac{k_T}{r+R'}\left[\frac{\partial T}{\partial r}+(r+R')\frac{\partial^2 T}{\partial r^2}\right]+\left(u\frac{\partial H}{\partial z}+v\frac{\partial H}{\partial r}\right)\mu_o T\frac{\partial m}{\partial T}$$
$$-\frac{k_T}{r+R'}\left(\frac{\partial q_r}{\partial r}(r+R')\right), \tag{6}$$

$$\frac{R'}{r+R'}u\frac{\partial C_1}{\partial z}+v\frac{\partial C_1}{\partial r}=D_{E_1}\frac{\partial^2 C_1}{\partial r^2}-k_1C_1C_2, \tag{7}$$

$$\frac{R'}{r+R'}u\frac{\partial C_2}{\partial z}+v\frac{\partial C_2}{\partial r}=D_{E_2}\frac{\partial^2 C_2}{\partial r^2}+k_1C_1C_2, \tag{8}$$

$$\left(\frac{R'}{r+R'}\right)u\frac{\partial N}{\partial z}+v\frac{\partial N}{\partial r}+\frac{\partial(N\tilde{v})}{\partial z}=D_m\frac{\partial^2 N}{\partial r^2}, \tag{9}$$

with boundary conditions

$$u=Az=U_w(z),\ \ v=0,\ -k_T\frac{\partial T}{\partial r}=h_1(T_w-T),\ D_{E_1}\frac{\partial C_1}{\partial r}=k_2C_1,$$
$$D_{E_2}\frac{\partial C_2}{\partial r}=-k_2C_1, N=N_w\ at\ \ r=0, \tag{10}$$

$$u\to 0,\quad \frac{\partial u}{\partial r}\to 0,\quad v\to 0,\quad T\to T_\infty,\quad C_1\to C_0,\quad C_2\to 0,\quad N\to N_\infty\quad as\quad r\to\infty, \tag{11}$$

where u and v are the velocity components in the radial ($z-$direction) and transverse ($r-$direction), respectively. A is the stretching constant, k_0 is the elasticity of Walter-B fluid, k_o^* is the porosity of porous medium, $Fr=\frac{C_b}{z\sqrt{k_o^*}}$ is the non-uniform inertia coefficient of porous medium in which C_b is the drag force, D_{E_1}, D_{E_2} are the diffusion coefficients, ρ is the fluid density, k_T is the thermal conductivity of fluid, σ is the electrical conductivity, μ is the dynamic viscosity, μ_o is the magnetic permeability, ρC_p is the heat capacity, D_m is the microorganisms diffusion, $\tilde{v}=\left(\frac{b_1W_{ce}}{\Delta C_1}\right)\frac{\partial C_1}{\partial r}$ is the average swimming velocity vector of the oxytactic microorganisms in which b_1 is the chemotaxis constant and W_{ce} is the maximum cell swimming speed [77, 80], T is the temperature and N is the gyrotactic microorganisms concentration. T_∞ and N_∞ stand for the temperature and motile microorganisms concentration density away from the surface, respectively, and h_1 denotes the convective heat transfer coefficient.

By Rosseland approximation [36], the radiative heat flux is defined as

$$q_r=-\frac{4\sigma^*}{3k^*}\frac{\partial T^4}{\partial r}, \tag{12}$$

where σ^* and k^* are the Stefan–Boltzmann constant and the mean absorption coefficient respectively. By using the supposition that the differences in heat transfer of the flow occur in such a way that T^4 can be written as a linear combination of the temperature, so implementing Taylor's theorem about T_∞ and ignoring the higher order terms, the result is

$$T^4=4T_\infty^3T-3T_\infty^4, \tag{13}$$

hence

$$\frac{\partial q_r}{\partial r}=-\frac{16T_\infty^3\sigma^*}{3k^*}\frac{\partial^2 T}{\partial r^2}. \tag{14}$$

2.1 | Magnetic dipole

The characteristics of the magnetic field have an effect on the flow of ferrofluid due to the magnetic dipole. Magnetic dipole effects are recognized by the magnetic scalar potential Φ as written in Equation (15)

$$\Phi = \frac{\gamma}{2\pi} \frac{z}{z^2 + (r+c)^2}, \tag{15}$$

where γ stands for the magnetic field strength at the source, c is the magnetic dipole distance from the center of the surface. By taking H_z and H_r as the components of magnetic field as written in Equations (16) and (17) as

$$H_z = -\frac{\partial \Phi}{\partial z} = \frac{\gamma}{2\pi} \frac{z^2 - (r+c)^2}{[z^2 + (r+c)^2]^2}, \tag{16}$$

$$H_r = -\frac{\partial \Phi}{\partial r} = \frac{\gamma}{2\pi} \frac{2z(r+c)}{[z^2 + (r+c)^2]^2}. \tag{17}$$

Due to the magnetic body, strength is usually proportional to the H_z and H_r gradient, it is therefore given in Equation (18) as

$$H = \sqrt{H_z^2 + H_r^2}. \tag{18}$$

Equation (19) can approximate the linear shape of magnetization m by temperature T as

$$m = K_1(T_c - T), \tag{19}$$

where K_1 is identified as the pyromagnetic coefficient.

Considering the following transformations [22, 74]

$$u = Azf'(\zeta), \quad v = -\left(\frac{R'}{r+R'}\right)\sqrt{A\nu} f(\zeta), \quad p = \rho A^2 z^2 P(\zeta), \quad \zeta = r\sqrt{\frac{A}{\nu}},$$
$$\theta(\zeta) = \frac{T - T_\infty}{T_w - T_\infty}, \quad C_1 = C_0\phi_1(\zeta), \quad C_2 = C_0\phi_2(\zeta), \quad \chi(\zeta) = \frac{N - N_\infty}{N_w - N_\infty}. \tag{20}$$

Using the transformations, Equations (4)– (11) are simplified as

$$p' = \frac{f'^2}{\zeta + \alpha_1}, \tag{21}$$

$$f''' + \frac{1}{\zeta+\alpha_1} f'' - \frac{1}{(\zeta+\alpha_1)^2} f' + \left(\frac{\alpha_1}{\zeta+\alpha_1}\right)\left[ff'' - f'^2 + \frac{1}{\alpha_1} f' f\right]$$
$$- \frac{\alpha}{(\zeta+\alpha_1)^2}\left[(2+\alpha_1)f'f'' - 2\alpha_1(ff'''' - f''^2)\right] - \alpha_2 f' - \alpha_3 f'^2 + \frac{2\beta}{(\zeta+d)^4}\theta + 2\left(\frac{\alpha_1}{\zeta+\alpha_1}\right)p = 0, \tag{22}$$

$$(1+Rd)\left(\theta'' + \frac{\theta'}{(\zeta+\alpha_1)}\right) + Pr\left(\frac{\alpha_1}{\zeta+\alpha_1}\right)f\theta' + \frac{2\beta Ec(\theta-\epsilon)f}{(\zeta+d)^3}$$
$$+ \beta Ec(\theta - \epsilon)\left[\frac{2f'}{(\zeta+d)^4} + \frac{4f}{(\zeta+d)^5}\right] = 0, \tag{23}$$

$$\phi_1'' + Sc\frac{\alpha_1}{(\zeta+\alpha_1)} f\phi_1' - Sck_3\phi_1\phi_2^2 = 0, \tag{24}$$

$$\delta\phi_2'' + Sc\frac{\alpha_1}{(\zeta+\alpha_1)} f\phi_2' + Sck_3\phi_1\phi_2^2 = 0, \tag{25}$$

$$\chi'' + Pe\left[\phi_1'\chi' + \phi_1''\chi + N_1\phi_1''\right] + Le\left(\frac{\alpha_1}{\zeta+\alpha_1}\right)f\chi' = 0, \tag{26}$$

with boundary conditions

$$f'(0) = 1, f(0) = 0, f(\infty) = 0, f''(\infty) = 0, \tag{27}$$

$$\theta'(0) = -Bi[1 - \theta(0)], \theta(\infty) = 0, \tag{28}$$

$$\phi_1'(0) = k_4\phi_1(0), \delta\phi_2'(0) = -k_4\phi_1(0), \phi_1(\infty) = 1, \phi_2(\infty) = 0, \tag{29}$$

$$\chi(0) = 1, \chi(\infty) = 0. \tag{30}$$

To eliminate the pressure term, integrating Equation (21) to get p and replacing it, so Equation (22) becomes

$$f''' + \frac{1}{\zeta + \alpha_1} f'' - \frac{1}{(\zeta + \alpha_1)^2} f' + \left(\frac{\alpha_1}{\zeta + \alpha_1}\right)\left[ff'' - f'^2 + \frac{1}{\alpha_1} f' f\right]$$
$$- \frac{\alpha}{(\zeta + \alpha_1)^2}\left[(2 + \alpha_1)f'f'' - 2\alpha_1(ff'''' - f''^2)\right] - \alpha_2 f' - \alpha_3 f'^2 + \frac{2\beta}{(\zeta + d)^4}\theta + \left(\frac{\alpha_1}{(\zeta + \alpha_1)^2}\right)(2ff'' - f'^2) = 0. \tag{31}$$

Many applications expect the diffusion coefficients E_1 and E_2 of the chemical species to be comparable in size, so leading to the assumption that the diffusion coefficients D_{E_1} and D_{E_2} are equal. The Chaudhar and Merkin concept is used [44], assuming $\delta = 1$ which provides the result as

$$\phi_1(\zeta) + \phi_2(\zeta) = 1. \tag{32}$$

Hence Eqs. (24) and (25) finally become

$$\phi_1'' + \frac{\phi_1'}{(\zeta + \alpha_1)} + Sc\frac{\alpha_1}{\zeta + \alpha_1} f\phi_1' - k_3\phi_1(1 - \phi_1)^2 = 0, \tag{33}$$

with boundary conditions as

$$\phi_1'(0) = k_4\phi_1(0), \phi_1(\infty) = 1, \tag{34}$$

where $\alpha_1 = R'\sqrt{\frac{A}{\nu}}$ is the curvature parameter, $\alpha_2 = \frac{\nu}{Ak_o^*}$ is the porosity parameter, $\alpha_3 = \frac{C_b}{\sqrt{k_o^*}}$ is the Forchheimer number, $\beta = \frac{\gamma\mu_o K_1 \rho(T_w - T_\infty)}{2\pi\mu^2}$ is the ferrohydrodynamic interaction parameter, $Pr = \frac{\mu C_p}{k_T}$ is the Prandtl number, $Ec = \frac{A\mu^2}{\rho(T_w - T_\infty)k_T}$ is the Eckert number, $d = \sqrt{\frac{Ac^2}{\nu}}$ is the dimensionless distance of magnetic dipole from the center of the surface, $\alpha = \frac{k_0 A}{\rho\nu}$ is the viscoelastic parameter, $Rd = \frac{16\sigma^* T_\infty^3}{3k_T k^*}$ is the thermal radiation parameter, $Sc = \frac{\nu}{D_{E_1}}$ is the Schmidt number, $Pe = \frac{bW_{ce}}{D_m}$ is the Peclet number, $Le = \frac{\nu}{D_m}$ is the Lewis number, $N_1 = \frac{N_\infty}{N_w - N_\infty}$ is the gyrotactic microorganisms concentration difference parameter, $Bi = \frac{h_1}{k_T}\sqrt{\frac{\nu}{A}}$ is the thermal Biot number, $k_3 = \frac{k_1 C_0^2}{A}$ is the strength of homogeneous chemical reaction parameter, $k_4 = k_2 Re^{-\frac{1}{2}}/D_{E_1}$ is the strength of heterogeneous chemical reaction parameter, $Re = \frac{A}{\nu}$ is the Reynolds number, and $\epsilon = \frac{T_\infty}{T_\infty - T_w}$ is the non-dimensional Curie temperature.

The interesting physical quantities, including skin friction coefficient, local Nusselt and motile density numbers, are accordingly given by

$$C_f = \frac{\tau_{rz}}{\rho(Az)^2},\ Nu_z = \frac{-zq_w}{k_T(T_w - T_\infty)},\ Sn_z = \frac{-zq_n}{D_m(N_w - N_\infty)}, \tag{35}$$

where τ_{rz} is the shear stress, q_w is heat flux and q_n is motile microorganisms flux at the wall and are defined as

$$\tau_{rz} = \mu u_r|_{r=0},\ q_w = -(k_T + \frac{16T_\infty^3\sigma^*}{3k^*})T_r|_{r=0},\ q_n = D_m N_r|_{r=0}. \tag{36}$$

So Equation (35) provide the result via Equation (36) as

$$C_f = \frac{1}{Re_z} f''(0),\ \ Nu = -Re_z^{0.5}(1+Rd)\theta'(0),\ \ Sn = -Re_z^{0.5}\chi'(0). \tag{37}$$

3 | SOLUTION METHODOLOGY

The suitable initial guesses are

$$f_0(\zeta) = (1-e^{-\zeta}),\ \ \theta_0(\zeta) = \frac{Bi}{1+Bi}e^{-\zeta},\ \ \phi_{1_0}(\zeta) = 1-e^{-\zeta},\ \ \chi_0 = e^{-\zeta}. \tag{38}$$

The auxiliary linear operators are

$$\mathbf{L}_f = f''' - f', \mathbf{L}_\theta = \theta'' - \theta, \mathbf{L}_{\phi_1} = {\phi_1}'' - \phi_1, \mathbf{L}_\chi = \chi'' - \chi. \tag{39}$$

Equations (38) and (39) satisfy the properties as given below

$$\begin{aligned} &L_f(Q_1 + Q_2e^{\zeta} + Q_3e^{-\zeta}) = 0,\ \ L_\theta(Q_4e^{\zeta} + Q_5e^{-\zeta}) = 0,\\ &L_{\phi_1}(Q_6e^{\zeta} + Q_7e^{-\zeta}) = 0,\ \ L_\chi(Q_8e^{\zeta} + Q_9e^{-\zeta}) = 0, \end{aligned} \tag{40}$$

where $Q_i(i = 1, \dots, 9)$ indicates the arbitrary constants.

The corresponding zeroth order form of the problems are

$$\begin{aligned} &(1-q)L_f[f(\zeta,q) - f_0(\zeta)] = qh_f\mathbf{N}_f[f(\zeta,q),\theta(\zeta,q)],\\ &(1-q)L_\theta[\theta(\zeta,q) - \theta_0(\zeta)] = qh_\theta\mathbf{N}_\theta[\theta(\zeta,q), f(\zeta,q)],\\ &(1-q)L_{\phi_1}[\phi_1(\zeta,q) - (\phi_1)_0(\zeta)] = qh_{\phi_1}\mathbf{N}_{\phi_1}[\phi_1(\zeta,q), f(\zeta,q)],\\ &(1-q)L_\chi[\chi(\zeta,q) - \chi_0(\zeta)] = qh_\chi\mathbf{N}_\chi[\chi(\zeta,q),\phi_1(\zeta,q), f(\zeta,q)], \end{aligned} \tag{41}$$

$$\begin{aligned} &f(0,q) = 0, f'(0,q) = 1,\ \ f''(\infty,q) = 0,\ \ \theta'(0,q) = -Bi(1-\theta(0,q)),\ \ \theta(\infty,q) = 0,\\ &\phi_1'(0,q) = k_4\phi_1(0,q), \phi_1(\infty,q) = 0,\ \ \chi(0,q) = 1,\ \ \chi(\infty,q) = 0, \end{aligned} \tag{42}$$

where

$$\begin{aligned} \mathbf{N}_f[f(\zeta,q),\theta(\zeta,q)] = {}& \frac{\partial^3 f(\zeta,q)}{\partial\zeta^3} + \frac{1}{\zeta+\alpha_1}\frac{\partial^2 f(\zeta,q)}{\partial\zeta^2} - \frac{1}{(\zeta+\alpha_1)^2}\frac{\partial f(\zeta,q)}{\partial\zeta}\\ &+ \left(\frac{\alpha_1}{\zeta+\alpha_1}\right)\left[f(\zeta,q)\frac{\partial^2 f(\zeta,q)}{\partial\zeta^2} - \left(\frac{\partial f(\zeta,q)}{\partial\zeta}\right)^2 + \frac{1}{\alpha_1}\frac{\partial f(\zeta,q)}{\partial\zeta}f(\zeta,q)\right] + \frac{\partial^2 f(\zeta,q)}{\partial\zeta^2}\frac{\partial^3 f(\zeta,q)}{\partial\zeta^3}\\ &- \frac{\alpha}{(\zeta+\alpha_1)^2}\left[(2+\alpha_1)\frac{\partial f(\zeta,q)}{\partial\zeta}\frac{\partial^2 f(\zeta,q)}{\partial\zeta^2} - \left(\frac{\partial f(\zeta,q)}{\partial\zeta}\right)^2 - 2\alpha_1\left(f(\zeta,q)\frac{\partial^3 f(\zeta,q)}{\partial\zeta^3} - \left(\frac{\partial^2 f(\zeta,q)}{\partial\zeta^2}\right)^2\right)\right]\\ &- \alpha_2\frac{\partial f(\zeta,q)}{\partial\zeta} - \alpha_3\left(\frac{\partial f(\zeta,q)}{\partial\zeta}\right)^2 + \frac{2\beta}{(\zeta+d)^4}\theta(\zeta,q) + \frac{\alpha_1}{(\zeta+\alpha_1)^2}\left(2f(\zeta,q)\frac{\partial^2 f(\zeta,q)}{\partial\zeta^2} - \left(\frac{\partial f(\zeta,q)}{\partial\zeta}\right)^2\right), \end{aligned} \tag{43}$$

$$\begin{aligned} \mathbf{N}_\theta[\theta(\zeta,q), f(\zeta,q)] = {}& (1+Rd)\left(\frac{\partial^2\theta(\zeta,q)}{\partial\zeta^2} + \frac{1}{(\zeta+\alpha_1)}\frac{\partial\theta(\zeta,q)}{\partial\zeta}\right) + Pr\left(\frac{\alpha_1}{\zeta+\alpha_1}\right)f(\zeta,q)\frac{\partial\theta(\zeta,q)}{\partial\zeta}\\ &+ \frac{2\beta Ec(\theta(\zeta,q)-\epsilon)f(\zeta,q)}{(\zeta+d)^3} + \beta Ec(\theta(\zeta,q)-\epsilon)\left[\frac{2}{(\zeta+d)^4}\frac{\partial f(\zeta,q)}{\partial\zeta} + \frac{4f(\zeta,q)}{(\zeta+d)^5}\right], \end{aligned} \tag{44}$$

$$\mathbf{N}_{\phi_1}[\phi_1(\zeta,q),f(\zeta,q)]=\frac{\partial^2\phi_1(\zeta,q)}{\partial\zeta^2}+\frac{1}{\zeta+\alpha_1}\frac{\partial\phi_1(\zeta,q)}{\partial\zeta}+Sc\frac{\alpha_1}{\zeta+\alpha_1}f(\zeta,q)\frac{\partial\phi_1(\zeta,q)}{\partial\zeta}-k_3\phi_1(\zeta,q)(1-\phi_1(\zeta,q))^2, \tag{45}$$

$$\mathbf{N}_{\chi}[\chi(\zeta,q),\phi_1(\zeta,q),f(\zeta,q)]=\frac{\partial^2\chi(\zeta,q)}{\partial\zeta^2}+Pe\left[\frac{\partial\phi(\zeta,q)}{\partial\zeta}\frac{\partial\chi(\zeta,q)}{\partial\zeta}+\frac{\partial^2\phi_1(\zeta,q)}{\partial\zeta^2}\chi(\zeta,q)+N_1\frac{\partial^2\phi_1(\zeta,q)}{\partial\zeta^2}\right]$$
$$+Le\left(\frac{\alpha_1}{\zeta+\alpha_1}\right)f(\zeta,q)\frac{\partial\chi(\zeta,q)}{\partial\zeta}, \tag{46}$$

where $q\in[0,1]$ is the embedding parameter, $\mathbf{N}_f$, $\mathbf{N}_\theta$, $\mathbf{N}_{\phi_1}$ and $\mathbf{N}_\chi$ are the nonlinear operators.

The mth order deformation problems is

$$L_f[f_m(\zeta,q)-\eta_m f_{m-1}(\zeta)]=h_f\mathcal{R}_f^m(\zeta), \tag{47}$$

$$L_\theta[\theta_m(\zeta,q)-\eta_m\theta_{m-1}(\zeta)]=h_\theta\mathcal{R}_\theta^m(\zeta), \tag{48}$$

$$\mathcal{L}_{\phi_1}[\phi_{1m}(\zeta,q)-\eta_m\phi_{1m-1}(\zeta)]=h_{\phi_1}\mathcal{R}_{\phi_1}^m(\zeta), \tag{49}$$

$$L_\chi[\chi_m(\zeta,q)-\eta_m\chi_{m-1}(\zeta)]=h_\chi\mathcal{R}_\chi^m(\zeta), \tag{50}$$

$$\begin{aligned}&f_m(0)=0,f_m'(0)=0,f_m'(\infty)=0,\\&\theta_m'(0)-Bi\theta_m(0)=0,\theta_m(\infty)=0,\\&{\phi_1}_m'(0)=k_4{\phi_1}_m(0),{\phi_1}_m(\infty)=0,\\&\chi_m(0)=0,\chi_m(\infty)=0,\end{aligned} \tag{51}$$

where

$$\eta_m=\begin{cases}0, & \text{if } m\le 1\\ 1, & \text{if } m>1,\end{cases} \tag{52}$$

while $\mathcal{R}_f^m(\zeta)$, $\mathcal{R}_\theta^m(\zeta)$, $\mathcal{R}_{\phi_1}^m(\zeta)$ and $\mathcal{R}_\chi^m(\zeta)$ are defined as

$$\mathcal{R}_f^m(\zeta)=f'''_{m-1}+\frac{1}{\zeta+\alpha_1}f''_{m-1}-\frac{1}{(\zeta+\alpha_1)^2}f'_{m-1}+\left(\frac{\alpha_1}{\zeta+\alpha_1}\right)\left[\sum_{r=0}^{m-1}f_{m-1-r}f''_r-\left(\sum_{r=0}^{m-1}f'_{m-1-r}f'_r\right)^2\right.$$
$$\left.+\frac{1}{\alpha_1}\sum_{r=0}^{m-1}f_{m-1-r}f'_r\right]-\frac{\alpha}{(\zeta+\alpha_1)^2}\left[(2+\alpha_1)\sum_{r=0}^{m-1}f'_{m-1-r}f''_r-2\alpha_1\left(\sum_{r=0}^{m-1}f_{m-1-r}f'''_r-\left(\sum_{r=0}^{m-1}f''_{m-1-r}f''_r\right)^2\right)\right]$$
$$-\alpha_2f'_{m-1}-\alpha_3\left(\sum_{r=0}^{m-1}f'_{m-1-r}f'_r\right)^2+\frac{2\beta}{(\zeta+d)^4}\theta_{m-1}+\left(\frac{\alpha_1}{(\zeta+\alpha_1)^2}\right)\left(2\sum_{r=0}^{m-1}f_{m-1-r}f''_r-\left(\sum_{r=0}^{m-1}f'_{m-1-r}f'_r\right)^2\right), \tag{53}$$

$$\mathcal{R}_\theta^m(\zeta)=(1+Rd)\left(\theta''_{m-1}+\frac{\theta'_{m-1}}{(\zeta+\alpha_1)}\right)+Pr\left(\frac{\alpha_1}{\zeta+\alpha_1}\right)\sum_{r=0}^{m-1}f_{m-1-r}\theta'_r$$
$$\frac{2\beta Ec(\theta_{m-1}-\epsilon)f_{m-1}}{(\zeta+d)^3}+\beta Ec(\theta_{m-1}-\epsilon)\left[\frac{2f'_{m-1}}{(\zeta+d)^4}+\frac{4f_{m-1}}{(\zeta+d)^5}\right], \tag{54}$$

$$\mathcal{R}_{\phi_1}^m(\zeta)=\phi''_{1\,m-1}+\frac{\phi'_{1m-1}}{(\zeta+\alpha_1)}+\left(\frac{\alpha_1}{\zeta+\alpha_1}\right)Sc\sum_{r=0}^{m-1}f_{m-1-r}\phi'_{1r}-Sc\phi_{1m-1}, \tag{55}$$

TABLE 1 Comparsion of the numerical results with [45].

α_1 (Curvature parameter)	Ashraf and Haq [45]	Present results
2	1.55656	1.55658
3	1.33770	1.33775
4	1.24482	1.24484
20	1.06205	1.06203
100	1.03113	1.03112
1000	1.02438	1.02438

$$\mathcal{R}_{\chi}^{m}(\zeta) = \chi''_{m-1} + Pe\left[\sum_{r=0}^{m-1} \phi'_{1\,m-1-r}\chi'_r + \sum_{r=0}^{m-1} \phi''_{1\,m-1-r}\chi_r + N_1\phi''_{1\,m-1}\right]$$
$$+ Le\left(\frac{\alpha_1}{\zeta+\alpha_1}\right)\sum_{r=0}^{m-1} f_{m-1-r}\chi'_r. \tag{56}$$

By solving the mth order, the general solutions are given by

$$f_m(\zeta) = f_m^*(\zeta) + Q_1 + Q_2e^{\zeta} + Q_3e^{-\zeta}, \tag{57}$$

$$\theta_m(\zeta) = \theta_m^*(\zeta) + Q_4e^{\zeta} + Q_5e^{-\zeta}, \tag{58}$$

$$\phi_{1\,m}(\zeta) = \phi_{1\,m}^{\;*}(\zeta) + Q_6e^{\zeta} + Q_7e^{-\zeta}, \tag{59}$$

$$\chi_m(\zeta) = \chi_m^*(\zeta) + Q_8e^{\zeta} + Q_9e^{-\zeta}, \tag{60}$$

where $f_m^*(\zeta)$, $\theta_m^*(\zeta)$, $\phi_{1\,m}^{\;*}(\zeta)$, and $\chi_m^*(\zeta)$ are the special solutions.

4 | COMPARSION OF THE PRESENT SOLUTION WITH THE PUBLISHED LITERATURE

The results of the present work are compared with the results of other investigators who used other methodologies for obtaining results or even simulated results. This is needed to place this work in perspective with other work in the field and provides more credibility for the present results. Table 1 is constructed to verify the numerical results of curvature parameter and skin friction coefficient.

5 | RESULTS AND DISCUSSION

Figure 2 is taken to examine the effect of curvature parameter α_1 on the velocity profile $f'(\zeta)$. It shows that the velocity of the fluid decreases with higher values of α_1. Figure 3 is used to analyze the performance of the ferromagnetic hydrodynamic interaction parameter β and the velocity profile. Due to the behavior of β, the velocity is increasing. Usually, the Lorentz forces are strong as β increases and consequently, the velocity increases on the curved surface. Figure 4 shows the velocity function and the elasticity parameter α which illuminates the viscoelasticity characteristics of the Walter-B fluid. Here, an increase in α results in an increase in the flow of Walter-B fluid. Higher fluid motion increases the thickness of the hydrodynamic boundary layer and therefore increases the velocity of the fluid. Figure 5 describes the nature of the porosity parameter α_2 and velocity $f'(\zeta)$ role. The present porous medium accelerates the flow field, resulting in a decrement in shear stress on the curved surface and, as a result, the velocity profile shows an increasing trend by increasing values of α_2. Figure 6 shows the effect of Darcy Forchheimer parameter α_3 on the velocity profile. It is clear that the velocity component decreases with the higher values of Darcy Forchheimer parameter α_3.

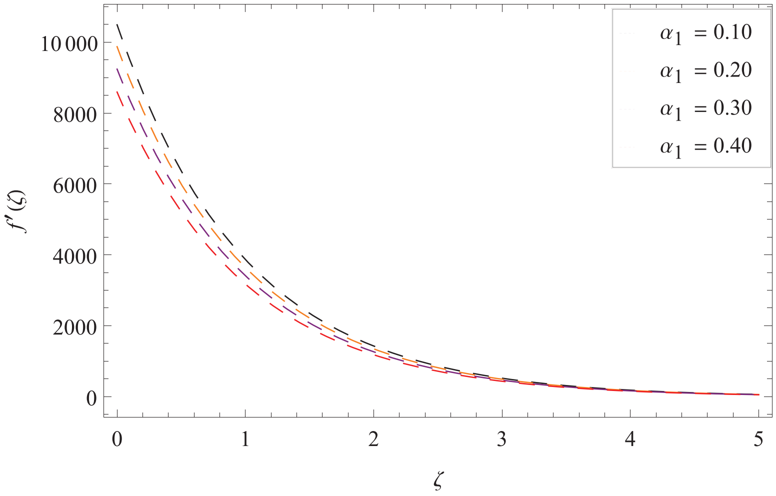

FIGURE 2 Influence of the parameter on the profile.

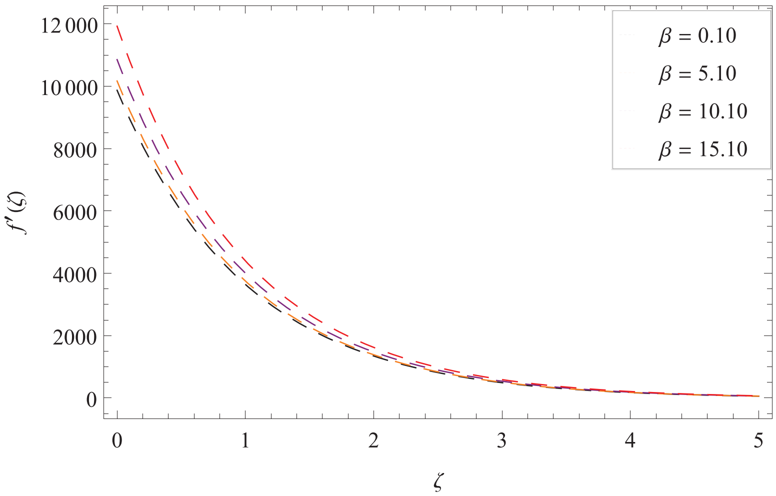

FIGURE 3 Influence of the parameter on the profile.

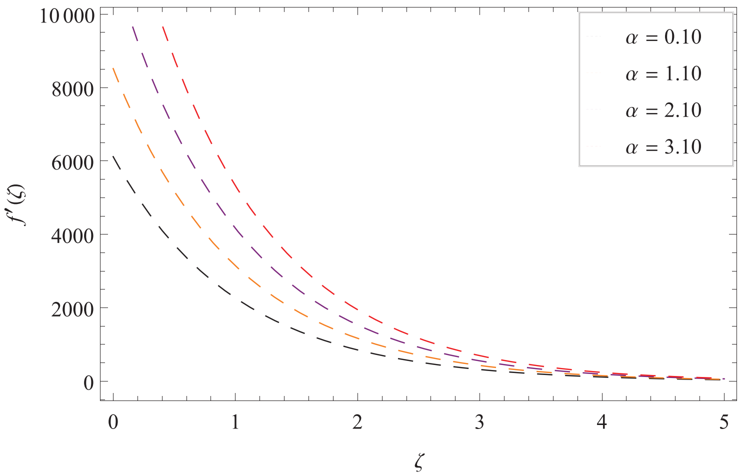

FIGURE 4 Influence of the parameter on the profile.

Figure 7 is used to show the effect of curvature parameter α_1 on the temperature profile $\theta(\zeta)$. It is clearly shown that the heat transfer decreases initially and then goes to increasing and finally resumes the same decreasing behavior. Figure 8 depicts the effect of ferromagnetic interaction parameter β on the temperature. The heat transfer increases with higher values of β. Figure 9 shows the temperature attributes of dimensionless Curie temperature parameter ε. Heat transfer decreases with the larger values of ε. Fluid thermal conductivity increases with the enhancements of ε. As a result, the extra heat is exchanged from the surface to the liquid and the temperature increases. Figure 10 shows the effect of elasticity

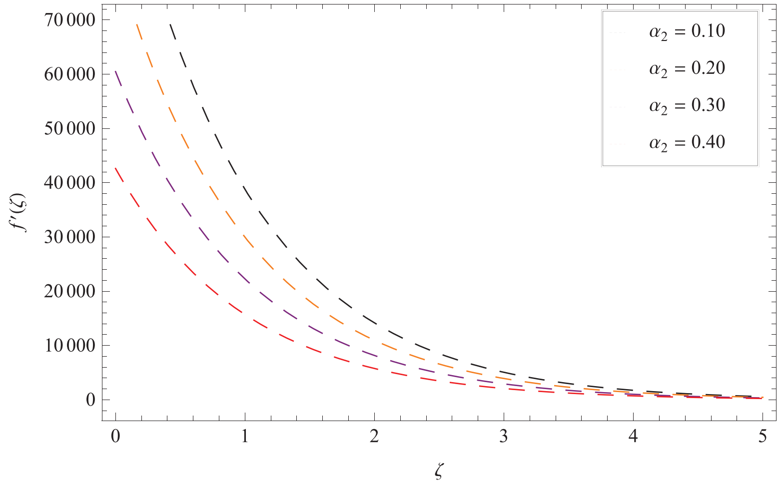

FIGURE 5 Influence of the parameter on the profile.

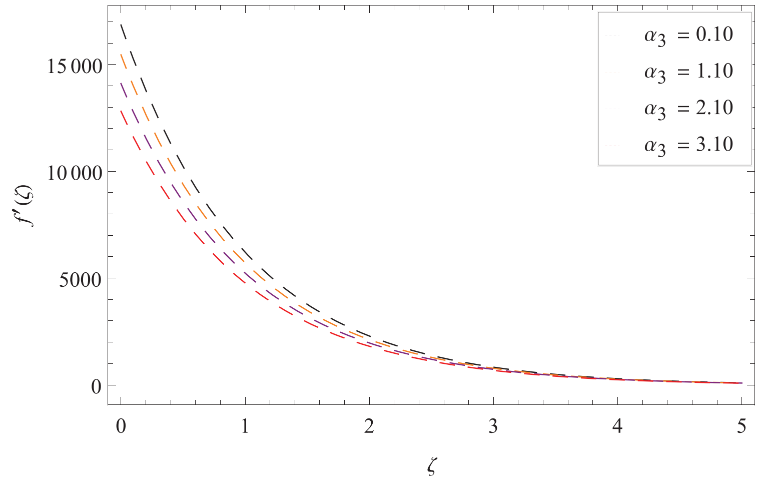

FIGURE 6 Influence of the parameter on the profile.

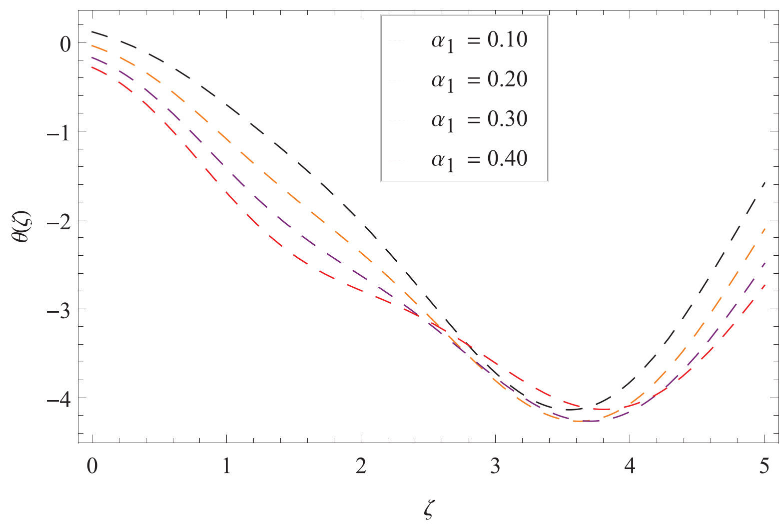

FIGURE 7 Influence of the parameter on the profile.

parameter α on temperature. The temperature decreases with an increase in α values. Physically thermal conductivity of liquid decays with larger values of α which reduces the heat transfer. Figure 11 shows the response of the thermal Biot number Bi and temperature profile $\theta(\zeta)$. It is noted that temperature is decreasing with a high values of Bi. Thermal Biot number Bi depends on the coefficient of heat transfer or, in other words, it is directly proportional to the coefficient of heat transfer. Figure 12 shows the temperature variations for the increasing values of Prandtl number Pr. The temperature

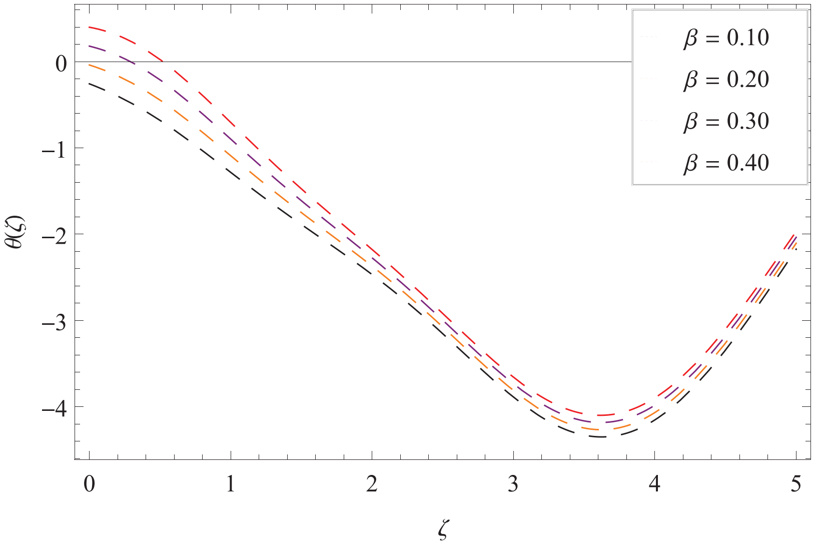

FIGURE 8 Influence of the parameter on the profile.

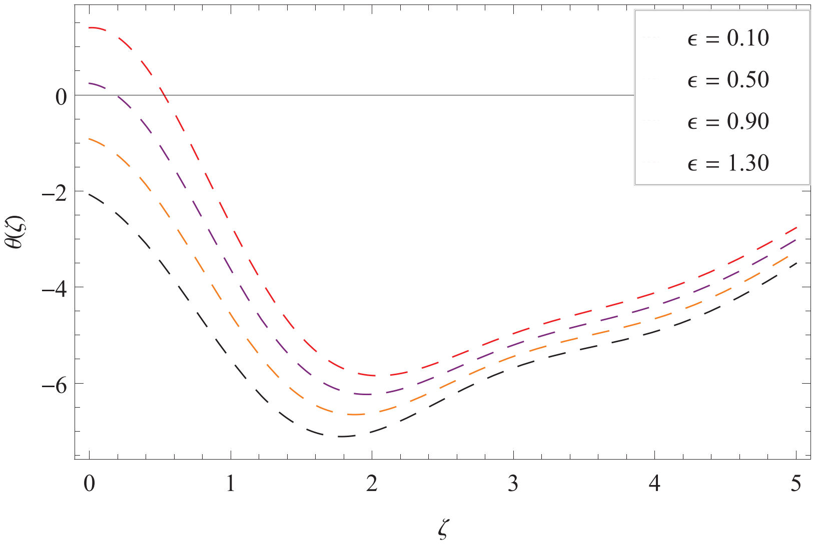

FIGURE 9 Influence of the parameter on the profile.

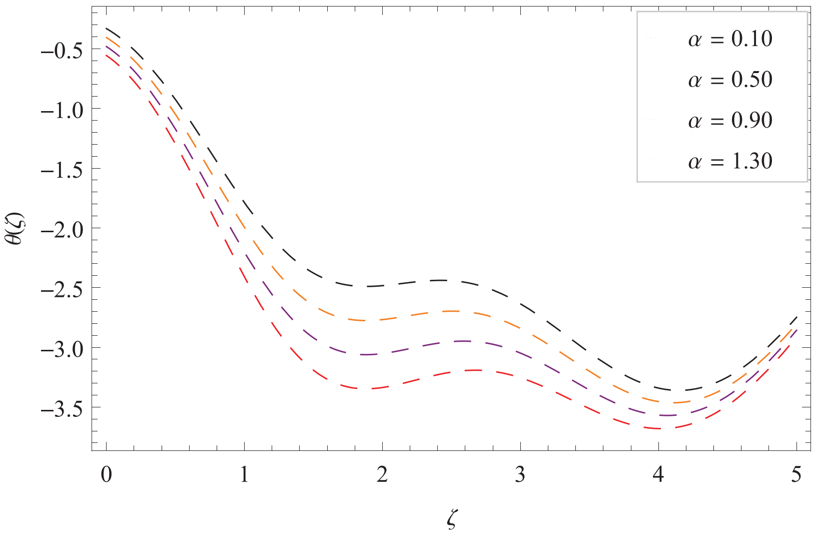

FIGURE 10 Influence of the parameter on the profile.

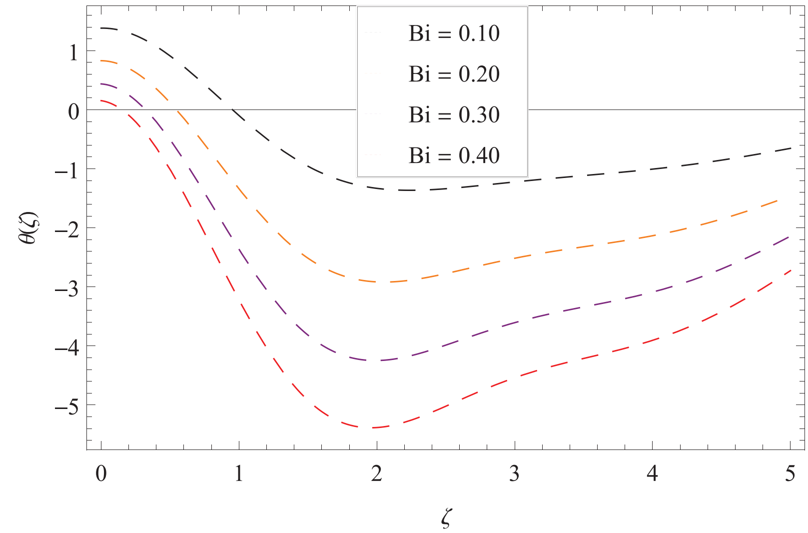

FIGURE 11 Influence of the parameter on the profile.

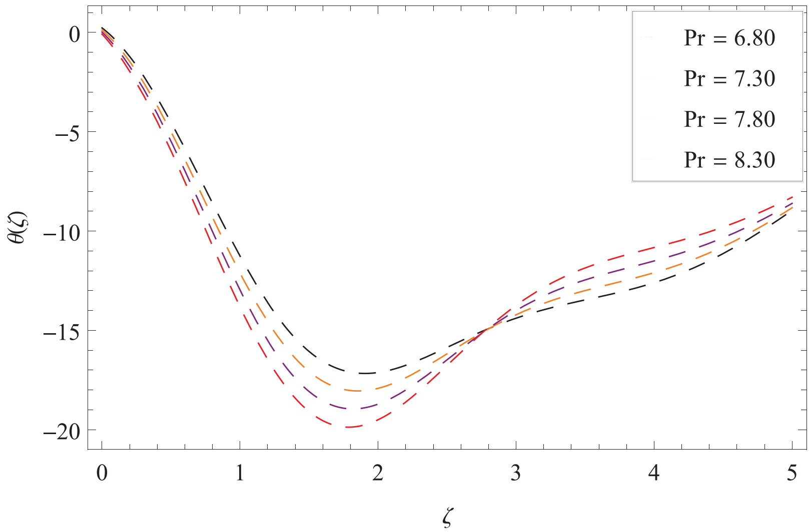

FIGURE 12 Influence of the parameter on the profile.

of the Walter-B fluid decreases with the higher values of Pr. Physically, Prandtl number refers to the thermal diffusivity. Larger Pr is related to the lower thermal diffusivity which causes the temperature to decompose. Figure 13 shows that the temperature of the fluid decreases due to the higher values of the thermal radiation parameter Rd. In this case, the absorption coefficient k^* decreases with an increase in Rd, which leads to decrease in the rate of radiative heat transfer.

Figure 14 is used to analyze the impact of the homogeneous reaction parameter k_3. It is noted that the concentration profile $\phi_1(\zeta)$ is increased with the larger values of k_3. Figure 15 shows the heterogeneous reaction parameter k_4 effect on concentration profile. The concentration of fluid decreases by increasing the values of k_4. Figure 16 shows the effect of Schmidt number Sc on the concentration profile. The concentration of the particles is increased by an increase in the Schmidt number. The effect of elasticity parameter α on concentration profile is shown through Figure 17. Strong Newtonian effect of the fluid enriches the concentration of homogeneous chemical reaction. It is evident from Figure 18 that the concentration of homogeneous chemical reaction $\phi_1(\zeta)$ is an increasing function of ferromagnetic interaction parameter β. Through dipole effect, the resistivity of the chemical reaction is enhanced which improves the homogeneous chemical reaction. Figure 19 portrays the influence of curvature parameter α_1 on the homogeneous chemical reaction $\phi_1(\zeta)$. It is observed that as the curvature increases, the space for concentration is expanded and hence the speed of concentration becomes slow.

Figure 20 presents the role of gyrotactic microorganism motion profile $\chi(\zeta)$ and the elasticity parameter α. It is evident that the concentration of motile microorganisms rises with the high values of α. The impact of ferromagnetic interaction parameter β is provided through Figure 21. It is seen that motile microorganisms motion on the curved sheet is enhanced with high values of β. Curvature parameter α_1 efficiency is clear from Figure 22. No doubt, when curvature is increased,

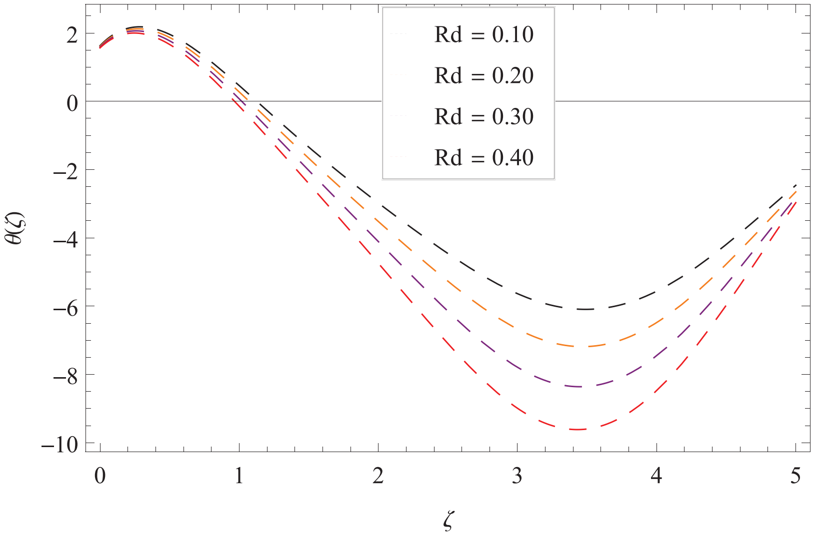

FIGURE 13 Influence of the parameter on the profile.

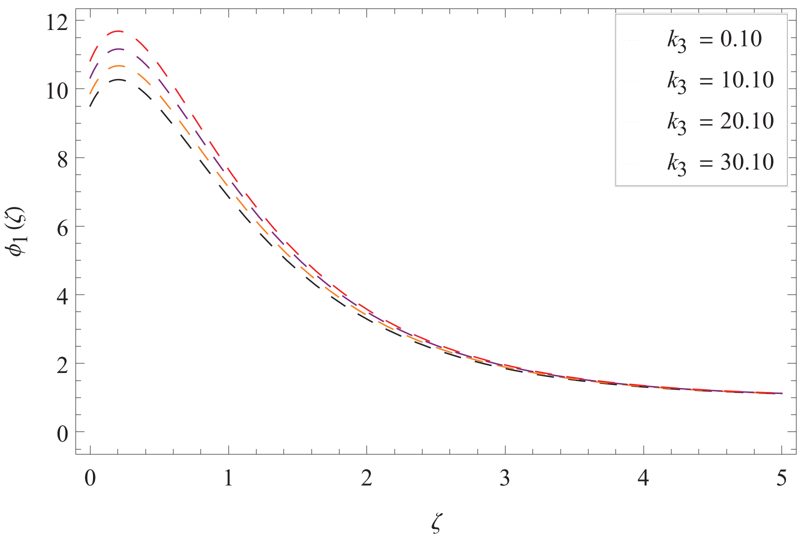

FIGURE 14 Influence of the parameter on the profile.

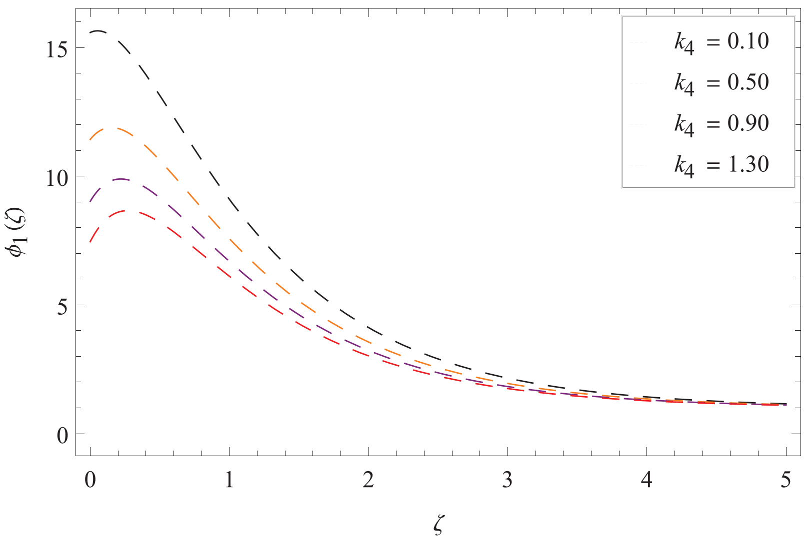

FIGURE 15 Influence of the parameter on the profile.

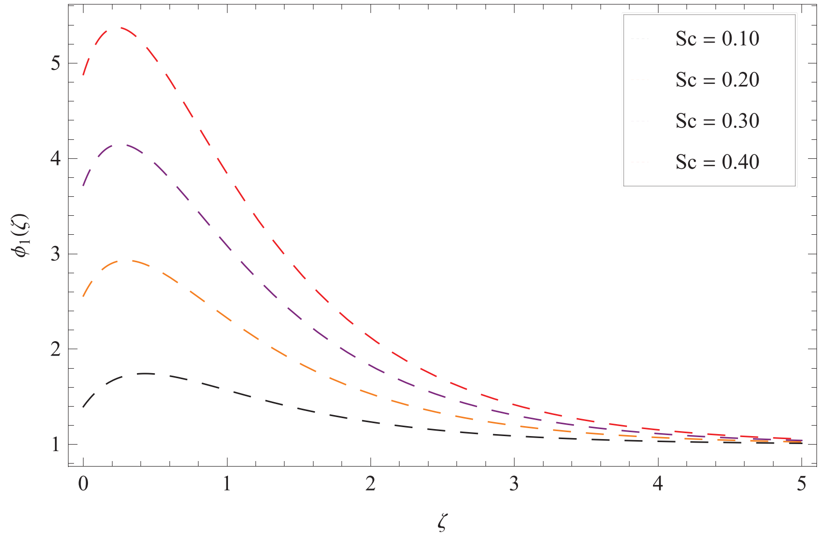

FIGURE 16 Influence of the parameter on the profile.

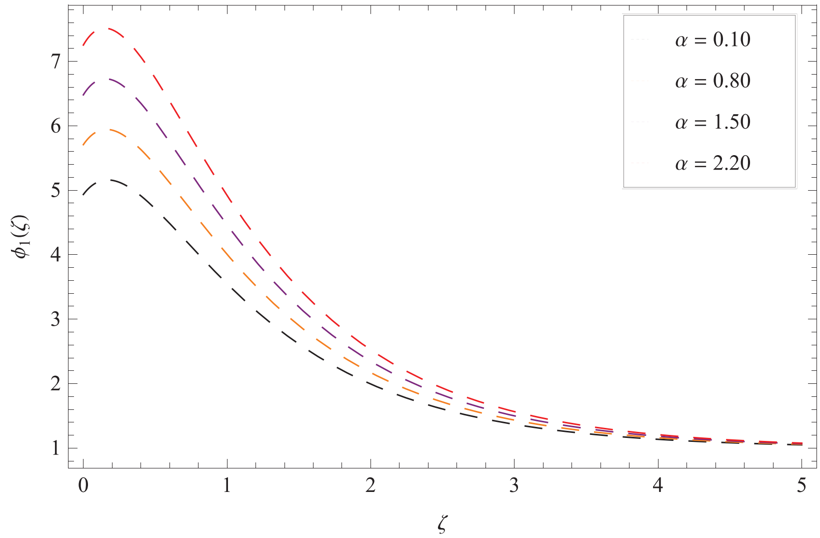

FIGURE 17 Influence of the parameter on the profile.

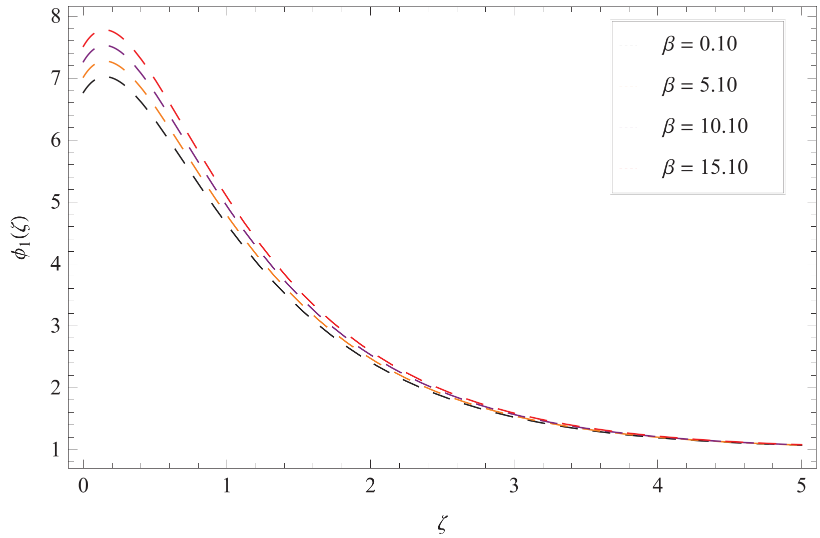

FIGURE 18 Influence of the parameter on the profile.

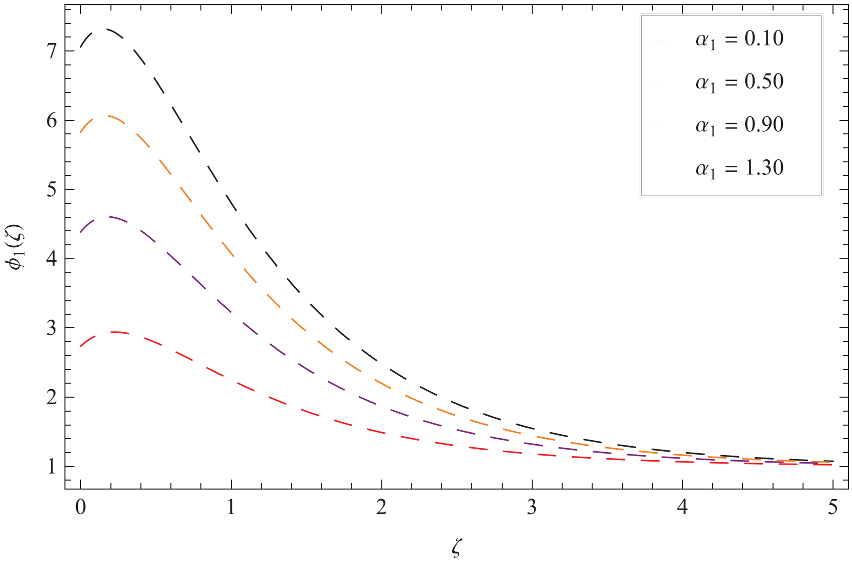

FIGURE 19 Influence of the parameter on the profile.

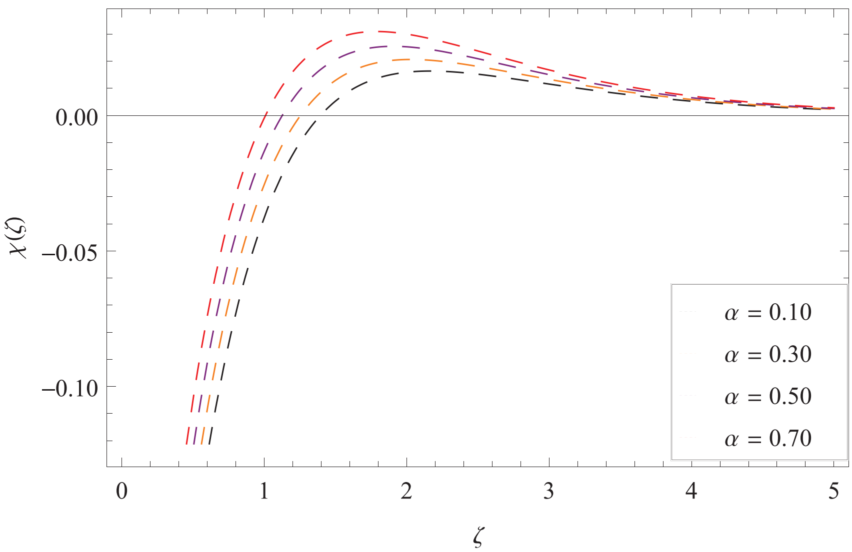

FIGURE 20 Influence of the parameter on the profile.

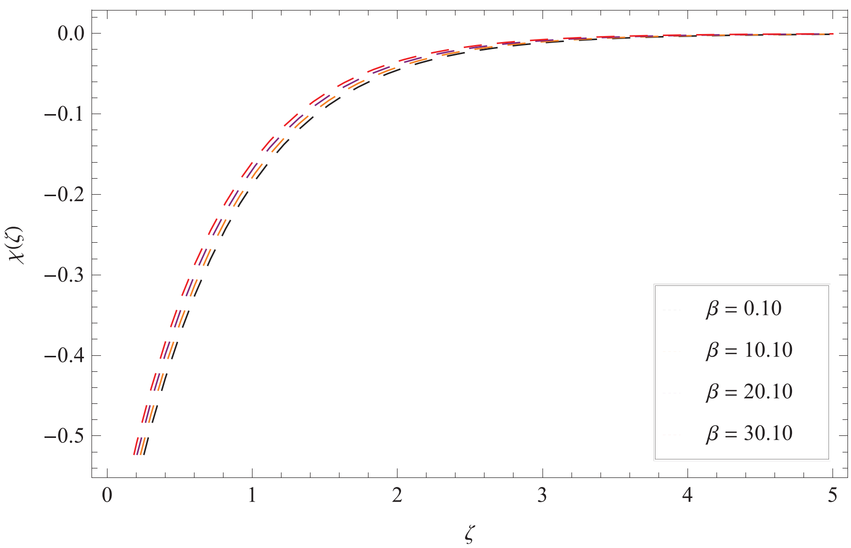

FIGURE 21 Influence of the parameter on the profile.

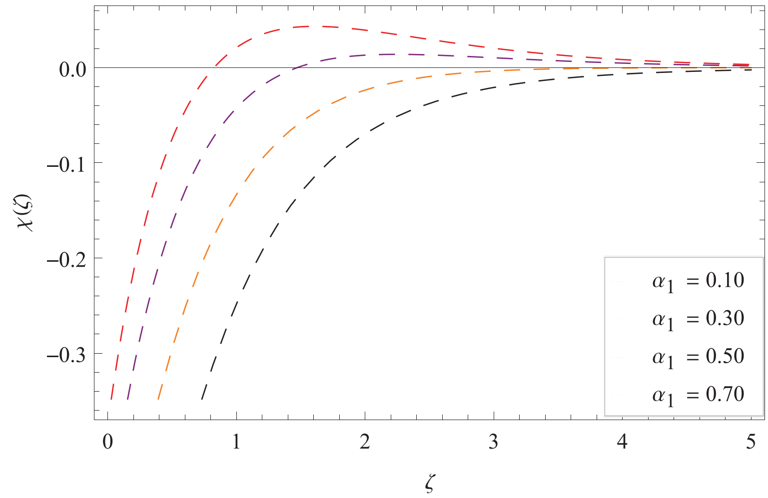

FIGURE 22 Influence of the parameter on the profile.

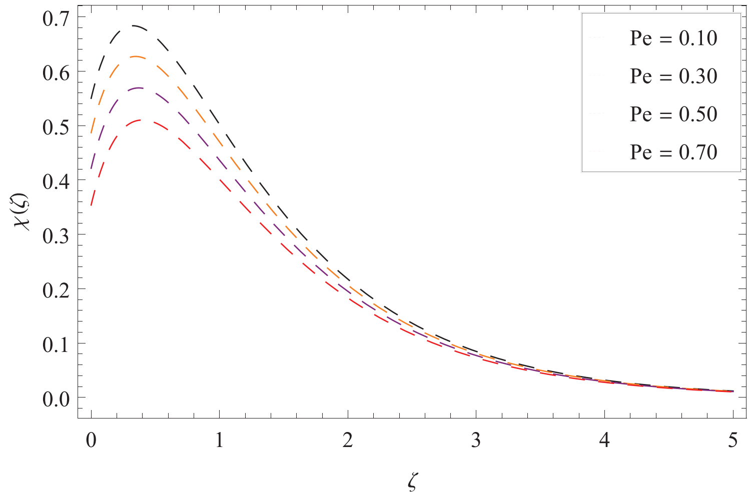

FIGURE 23 Influence of the parameter on the profile.

the microorganisms motion is automatically increased. Figure 23 shows the effect of Peclet number *Pe* on the microorganisms profile $\chi(\zeta)$. There is a clear reason for the decreased density of the microorganisms due to the increment in *Pe* which is evident from Equation (26). Figure 24 reports the effect of Lewis number *Le* on the microorganisms profile. The increase in the microorganisms distribution is noted because the Lewis number is directly proportional to the microorganisms diffusion.

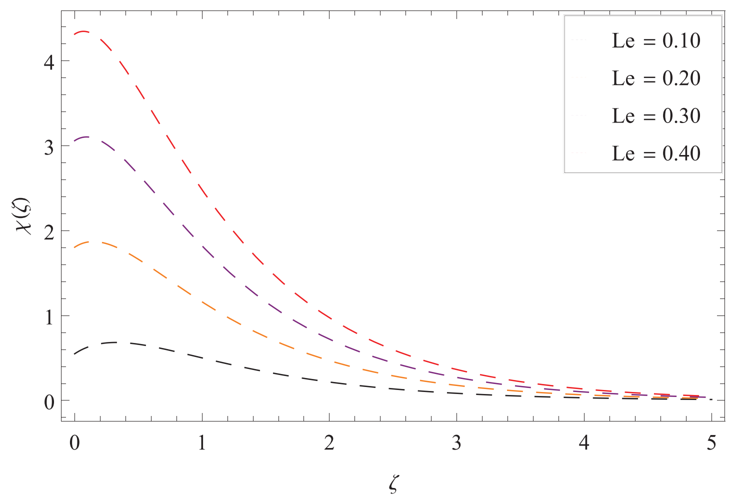

FIGURE 24 Influence of the parameter on the profile.

6 | CONCLUSION

A mathematical model of homogeneous heterogeneous chemical reactions is proposed to investigate the hydromagnetic flow of Walter-B fluid through a porous medium past a curved stretching sheet with thermal radiation in the presence of magnetic dipole. The resulting non-dimensional differential equations are achieved after the application of similarity transformations for which the solution is obtained analytically. The main points are as follows

- Velocity is declined with the increasing values of curvature parameter α_1, porosity parameter α_2, Darcy–Forchheimer parameter α_3 and it increases with the high values of ferromagnetic parameter β and elasticity parameter α.
- Temperature decreases with increasing values of curvature parameter α_1, elasticity parameter α, thermal Biot number Bi, thermal radiation parameter Rd, and Prandtl number Pr while it increases with ferromagnetic parameter β and Curie temperature parameter ε.
- Larger heterogeneous reaction parameter k_4 and curvature parameter α_1 portray a reduction in the concentration rate of chemical reactions, while higher homogeneous reaction parameter k_3, elasticity parameter α, ferromagnetic parameter β, and Schmidt number Sc lead to a higher rate of homogeneous chemical reaction concentration.
- Density of the gyrotactic microorganisms increases with the high values of elasticity parameter α, ferromagnetic parameter β, curvature parameter α_1 and Lewis number Le while it decreases with the Peclet number Pe.

NOMENCLATURE

m	magnetization
A	stretching constant
(u, v)	velocity components
$\tilde{\upsilon}$	average swimming velocity of oxytactic microorganisms
W_{ce}	cell swimming speed
ν	kinematic viscosity
(r, z)	curvilinear coordinates
β	ferromagnetic parameter
k^*	mean absorption coefficient
K_1	pyromagnetic coefficient
k_1, k_2	chemical reactant rate constants
k_T	thermal conductivity
k_3	homogeneous chemical reaction parameter
k_4	heterogeneous chemical reaction parameter
ρ	density
μ_0	magnetic permeability
μ	dynamic viscosity
H	magnetic field
P	pressure
Bi	thermal Biot number
E_1	chemical reactant
E_2	chemical reactant
C_1	concentration of chemical reactant E_1
C_2	concentration of chemical reactant E_2
q_r	radiative heat flux
Rd	thermal radiation parameter
Re	Reynolds number
σ^*	Stefan–Botlzmann constant
D_{E_1}, D_{E_2}	diffusion coefficients
D_m	mass diffusion coefficient
b_1	chemotaxis constant
k^*	mean absorption coefficient

δ	ratio of diffusion coefficients
T	temperature
N	microorganisms density
Fr	inertial coefficient
c	magnetic dipole distance from the center of the surface
C_P	specific heat at constant pressure
C_b	drag force
ζ	similarity variable
$f'(\zeta)$	dimensionless velocity
$\theta(\zeta)$	dimensionless temperature
$\phi_1(\zeta)$	dimensionless homogeneous chemical concentration
$\phi_2(\zeta)$	dimensionless heterogeneous chemical concentration
$\chi(\zeta)$	dimensionless gyrotactic microorganisms concentration
ϵ	Curie temperature
Pr	Prandtl number
γ	magnetic field strength
d	dimensionless distance of magnetic dipole from the center of the surface
Φ	magnetic potential
Le	bioconvection Lewis number
Pe	bioconvection Peclet number
α	elasticity parameter
α_1	curvature parameter
α_2	porosity parameter
Ec	Eckert number
α_3	Darcy–Forchhemier parameter
$'$	differentiation with respect to ζ

ACKNOWLEDGMENTS

The authors are thankful to the respectable reviewers for their comments and suggestions. The authors acknowledge the financial support provided by the Center of Excellence in Theoretical and Computational Science (TaCS-CoE), KMUTT. This research was funded by National Science, Research and Innovation Fund (NSRF), King Mongkut's University of Technology North Bangkok with Contract no. KMUTNB-FF-66-61. The first author is thankful to the Higher Education Commission (HEC) Pakistan for providing the technical and financial support through the Startup Research Grant Program (SRGP) under project no. 10534.

CONFLICT OF INTEREST

The authors have no conflict of interests.

ORCID

Noor Saeed Khan https://orcid.org/0000-0003-0991-7846
Wiyada Kumam https://orcid.org/0000-0001-8773-4821
Poom Kumam https://orcid.org/0000-0002-5463-4581

REFERENCES

[1] Andersson, H., Valnes, O.: Flow of a heated ferrofluid over a stretching sheet in the presence of a magnetic dipole. Acta. Mech. 128(1-2), 39–47 (1998)
[2] Ali, B., Siddique, I., Khan, I., Masood, B., Hussain, S.: Magnetic dipole and thermal radiation effects on hybrid base micropolar CNTs flow over a stretching sheet: finite element method approach. Result. Phys. 25, 104145 (2021)
[3] Alfannakh, H.: Significances of magnetic dipole flow and melting heat transfer over suspended dust particles along with carbon nanotubes. Front. Energy Res. 10, 935108 (2022)
[4] Waqas, H., Hussain, M., Alqarni, M.S., Eid, M.R., Muhammad, T.: Numerical simulation for magnetic dipole in bioconvection flow of Jeffery nanofluid with swimming motile microorganisms. Waves in Random and Complex Media (2021)

[5] Bashir, S., Ramzan, M., Ghazwani, H.A.S., Nisar, K.S., Saleel, C.A., Abdelrahman, A.: Magnetic dipole and thermophoretic particle deposition impact on bioconvection Oldroyd-B fluid flow over a stretching surface with Cattaneo-Christov heat flux. Nanomat. 12, 2181 (2022)

[6] Souayeh, B., Yasin, E., Alam, M.W., Hussain, S.G.: Numerical simulation of magnetic dipole flow over a stretching sheet in the presence of non-uniform heat source/sink. Front. Energy Res. 9, 767751 (2021)

[7] Sajjad, R., Mushtaq, M., Farid, S., Jabeen, K., Muntazir, R.M.A.: Numerical simulations of magnetic dipole over a nonlinear radiative Eyring-Powell nanofluid considering viscous and Ohmic dissipation effects. Math. Prob. Eng. 2021, 9776759 (2021)

[8] Gowda, R.J.P., Kumar, R.N., Prasannakumara, B.C., Nagaraja, B., Gireesha, B.J.: Exploring magnetic dipole contribution on ferromagnetic nanofluid flow over a stretching sheet: an application of Stefan blowing. J. Mol. Liquids 335, 116215 (2021)

[9] Kumar, K.G.: Impact of magnetic dipole on flow and heat transfer of AA7072-AA7075/water based nanofluid over a stretching sheet using Koo and Kleinstreuer model. Eur. Phys. J. Plus. 137, 669 (2022)

[10] Khan, N.S., Zuhra, S., Shah, Q.: Entropy generation in two phase model for simulating flow and heat transfer of carbon nanotubes between rotating stretchable disks with cubic autocatalysis chemical reaction. Appl. Nanosci. 9, 1797–1822 (2019)

[11] Khan, N.S., Shah, Q., Bhaumik, A., Kumam, P., Thounthong, P., Amiri, I.: Entropy generation in bioconvection nanofluid flow between two stretchable rotating disks. Sci. Rep. 10, 4448 (2020)

[12] Usman, A.H., Khan, N.S., Humphries, U.W., Ullah, Z., Shah, Q., Kumam, P., Thounthong, P., Khan, W., Kaewkhao, A., Bhaumik, A.: Computational optimization for the deposition of bioconvection thin Oldroyd-B nanofluid with entropy generation. Sci. Rep. 11(1), 1164 (2021)

[13] Khan, N.S., Shah, Z., Islam, S., Khan, I., Alkanhal, T.A., Tlili, I.: Entropy generation in MHD mixed convection non-Newtonian second-grade nanoliquid thin film flow through a porous medium with chemical reaction and stratification. Entropy 21, 139 (2019)

[14] Khan, N.S., Zuhra, S., Shah, Z., Bonyah, E., Khan, W., Islam, S., Khan, A.: Hall current and thermophoresis effects on magnetohydrodynamic mixed convective heat and mass transfer thin film flow. J. Phys. Commun. 3, 035009 (2019)

[15] Khan, N.S., Kumam, P., Thounthong, P.: Magnetic field promoted irreversible process of water based nanocomposites with heat and mass transfer flow. Sci. Rep. 1, 11692 (2021)

[16] Khan, N.S., Kumam, P., Thounthong, P.: Renewable energy technology for the sustainable development of thermal system with entropy measures. Int. J. Heat Mass Transf. 145, 118713 (2019)

[17] Khan, N.S., Shah, Q., Sohail, A., Kumam, P., Thounthong, P., Muhammad, T.: Mechanical aspects of Maxwell nanofluid in dynamic system with irreversible analysis. ZAMM J. Appl. Math. Mech. Z. Angewwandte Math. Mech. e202000212 (2021)

[18] Usman, A.H., Khan, N.S., Rano, S.A., Humphries, U.W., Kumam, P.: Computational investigations of Arrhenius activation energy and entropy generation in a viscoelastic nanofluid flow thin film sprayed on a stretching cylinder. J. Adv. Res. Fluid Mech. Therm. Sci. 86(1), 27–51 (2021)

[19] Reddy, M.G., Sudharani, M.V.V.N.L., Praveena, M.M., Kumar, K.G.: Effect of thermal conductivity on Blasius-Rayleigh-Stokes flow and heat transfer over a moving plate by considering magnetic dipole moment. Eur. Phys. J. Plus. 137, 29 (2022)

[20] Gowda, R.J.P., Jyothi, A.M., Kumar, R.N., Prasannakumara, B.C., Sarris, I.E.: Convective flow of second grade fluid over a curved stretching sheet with Dufour and Soret effects. Int. J. Appl. Comput. Math. 7, 226 (2021)

[21] Babu, B.H., Rao, P.S., Reddy, M.G.: Physical aspects and streamline analysis on hydromagnetic nonlinear radiative flow of Carreau-Yasuda fluid. Phys. Scr. 96, 025221 (2020)

[22] Sheikholeslami, M., Jafaryar, M., Said, Z., Alsabery, A.I., Babazadeh, H., Shafee, A.: Modification for helical turbulator to augment heat transfer behavior of nanomaterial via numerical approach. Appli. Therm. Eng. (2020)

[23] Tripathi, D., Prakash, J., Reddy, M.G., Kumar, R.: Numerical study of electroosmosis-induced alterations in peristaltic pumping of couple stress hybrid nanofluids through microchannel. Indian J. Phys. 95(11), 2411–2421 (2021)

[24] Sheikholeslami, M., Farshad, S.A., Ebrahimpour, Z., Said, Z.: Recent progress on flat plate solar collectors and photovoltaic systems in the presence of nanofluid: a review. J. Cleaner Prod. 293, 126119 (2021)

[25] Reddy, M.G., Kumar, R.: Cattaneo-Christov heat flux feature on carbon nanotubes filled with micropolar liquid over a melting surface: a stream line study. Int. Commun. Heat Mass Transf. 122, 105142 (2021)

[26] Sheikholeslami, M., Farshad, S.A., Said, Z.: Analyzing entropy and thermal behavior of nanomaterial through solar collector involving new tapes. Int. Commun. Heat Mass Transf. 123, 105190 (2021)

[27] Reddy, M.G., Rani, M.V.V.N.L.S., Kumar, K.G., Prasannakumar, B.C., Chamkha, A.J.: Cattaneo-Christov heat flux model on Blasius-Rayleigh-Stokes flow through a transitive magnetic field and Joule heating. Phys. A: Stat. Mech. Appl. 548, 123991 (2020)

[28] Sheikholeslami, M., Farshad, S.A.: Investigation of solar collector system with turbulator considering hybrid nanoparticles. Renew. Energy. 171, 1128-1158 (2021)

[29] Shehzad, S.A., Reddy, M.G., Rauf, A., Abbas, Z.: Bioconvection of Maxwell nanofluid under the influence of double diffusive Cattaneo-Christov theories over isolated rotating disk. Phys. Scr. 95, 045207 (2020)

[30] Devi, S.V.V.R., Reddy, M.G.: Parametric analysis of MHD flow of nanofluid in stretching sheet under chemical sensitivity and thermal radiation. Heat Transf. 51, 94–975 (2022)

[31] Reddy, M.G., Rani, M.V.V.N.L.S., Praveena, M.M., Kumar, K.G.: Comparative study of different non-Newtonian fluid over an elaborated sheet in the view of dual stratified flow and ohmic heat. Chem. Phys. Letters. 784, 139096 (2021)

[32] Reddy, M.G., Rrani, M.V.V.N.L.S., Kumar, K.G., Prasannakumara, B.C.: Cattaneo-Christov heat flux and non-uniform heat source/sink impacts on radiative Oldroyd-B two-phase flow across a cone/wedge. J. Braz. Soc. Mech. Sci. Eng. 40, 95 (2018)

[33] Megahed, A.M., Reddy, M.G., Abbas, W.: Modeling of MHD fluid flow over an unsteady stretching sheet with thermal radiation, variable fluid properties and heat flux. Math. Comp. Sim. 185, 583–593 (2021)

[34] Khan, N.S.: Bioconvection in second grade nanofluid flow containing nanoparticles and gyrotactic microorganisms. Braz. J. Phys. 43, 227–241 (2018)

[35] Khan, N.S., Gul, T., Khan, M.A., Bonyah, E., Islam, S.: Mixed convection in gravity-driven thin film non-Newtonian nanofluids flow with gyrotactic microorganisms. Result. Phys. 7, 4033–4049 (2017)

[36] Khan, N.S., Gul, T., Islam, S., Khan, W.: Thermophoresis and thermal radiation with heat and mass transfer in a magnetohydrodynamic thin film second-grade fluid of variable properties past a stretching sheet. Eur. Phys. J. Plus 32, 11 (2017)

[37] Palwasha, Z., Khan, N.S., Shah, Z., Islam, S., Bonyah, E.: Study of two dimensional boundary layer thin film fluid flow with variable thermo-physical properties in three dimensions space. AIP Adv. 8, 105318 (2018)

[38] Khan, N.S., Gul, T., Islam, S., Khan, A., Shah, Z.: Brownian motion and thermophoresis effects on MHD mixed convective thin film second-grade nanofluid flow with Hall effect and heat transfer past a stretching sheet. J. Nanofluids 6, 812–829 (2017)

[39] Khan, N.S., Zuhra, S., Shah, Z., Bonyah, E., Khan, W., Islam, S.: Slip flow of Eyring-Powell nanoliquid film containing graphene nanoparticles. AIP Adv. 8, 115302 (2019)

[40] Khan, N.S., Gul, T., Kumam, P., Shah, Z., Islam, S., Khan, W., Zuhra, S., Sohail, A.: Influence of inclined magnetic field on Carreau nanoliquid thin film flow and heat transfer with graphene nanoparticles. Energies 12(8), 1459 (2019)

[41] Khan, N.S.: Study of two dimensional boundary layer flow of a thin film second grade fluid with variable thermo-physical properties in three dimensions space. Filomat 33, 5387–5405 (2019)

[42] Khan, N.S., Zuhra, S.: Boundary layer flow and heat transfer in a thin film second grade nanoliquid embedded with graphene nanoparticles. Adv. Mech. Eng. 11(11), 1–11 (2019)

[43] Usman, A.H., Khan, N.S., Humphries, U.W., Shah, Z., Kumam, P., Khan, W., Khan, A., Rano, S.A., Ullah, Z.: Development of dynamic model and analytical analysis for the diffusion of different species in non-Newtonian nanofluid swirling flow. Front. Phys. 8, 616790 (2021)

[44] Merkin, J.H.: A model for isothermal homogeneous-heterogeneous reactions in boundary-layer flow. Math. Comp. Model. 24(8), 125–136 (1996).

[45] Ashraf, M.B., Haq, S.Ul: The convective flow of Carreau fluid over a curved stretching surface with homogeneous-heterogeneous reactions and viscous dissipation. Waves Random Complex Media (2022)

[46] Jawad, M., Saeed, A., Gul, T., Khan, A.: The magnetohydrodynamic flow of a nanofluid over a curved exponentially stretching surface. Heat Transf. 50, 5356–5379 (2021)

[47] Abbas, Z., Naveed, M., Sajid, M.: Heat transfer analysis for stretching flow over a curved surface with magnetic field. J. Eng. Thermophys. 22(4), 337–345 (2013)

[48] Hayat, T., Haider, F., Muhammad, T., Alsaedi, A.: Darcy-Forchheimer flow due to a curved stretching surface with Cattaneo-Christov double diffusion: a numerical study. Result. Phys. 7, 2663–2670 (2017)

[49] Raza, Rabeeha., Mabood, F., Naz, R., Abdelsalam, S.I.: Thermal transport of radiative Williamson fluid over stretchable curved surface. Therm. Sci. Eng. Progress 23, 100887 (2021)

[50] Abbas, Z., Naveed, M., Sajid, M.: Hydromagnetic slip flow of nanofluid over a stretching surface with heat generation and thermal radiation. J. Mol. Liquids. 215, 756–762 (2016)

[51] Muhammad, T., Rafique, K., Asma, M., Alghamdi, M.: Darcy-Forchheimer flow over an exponentially stretching curved surface with Cattaneo-Christov double diffusion. Phys. A: Stat. Mech. Appl. 556, 123968 (2020)

[52] Waqas, H., Bukhari, F.F., Farooq, U., Alqarni, M.S., Muhammad, T.: Numerical computation of melting heat transfer in nonlinear radiative flow of hybrid nanofluids due to permeable stretching curved surface. Case Studies Therm. Eng. 27, 101348 (2021)

[53] Khan, N.S., Gul, T., Islam, S., Khan, I., Alqahtani, A.M., Alshomrani, A.S.: Magnetohydrodynamic nanoliquid thin film sprayed on a stretching cylinder with heat transfer. J. Appl. Sci. 7, 271 (2017)

[54] Khan, N.S., Kumam, P., Thounthong, P.: Computational approach to dynamic systems through similarity measure and homotopy analysis method for renewable energy. Crystals 10(12), 1086 (2020)

[55] Khan, N.S., Shah, Q., Sohail, A., Kaewkhao, A., Kumam, P., Zubair, S., Ullah, N., Thounthong, P.: Rotating flow assessment of magnetized mixture fluid suspended with hybrid nanoparticles and chemical reactions of species. Sci. Rep. 11(1), 11277 (2021)

[56] Zuhra, S., Khan, N.S., Khan, M.A., Islam, S., Khan, W., Bonyah, E.: Flow and heat transfer in water based liquid film fluids dispensed with graphene nanoparticles. Result. Phys. 8, 1143–1157 (2018)

[57] Khan, N.S., Usman, A.H., Sohail, A., Hussanan, A., Shah, Q., Ullah, N., Kumam, P., Thounthong, P., Humphries, U.W.: A framework for the magnetic dipole effect on the thixotropic nanofluid flow past a continuous curved stretched surface. Crystals 11, 645 (2021)

[58] Khan, N.S., Usman, A.H., Kaewkhao, A., Kumam, P., Thounthong, P., Humphries, U.W.: Exploring the nanomechanical concepts of development through recent updates in magnetically guided system. Sci. Rep. 11(1), 13576 (2021)

[59] Khan, N.S., Gul, T., Islam, S., Khan, W., Khan, I., Ali, L.: Thin film flow of a second-grade fluid in a porous medium past a stretching sheet with heat transfer. Alex. Eng. J. 57, 1019–1031 (2017)

[60] Zuhra, S., Khan, N.S., Alam, A., Islam, S., Khan, A.: Buoyancy effects on nanoliquids film flow through a porous medium with gyrotactic microorganisms and cubic autocatalysis chemical reaction. Adv. Mech. Eng. 12(1), 1–17 (2020)

[61] Palwasha, Z., Islam, S., Khan, N.S., Ayaz, H.: Non-Newtonian nanoliquids thin film flow through a porous medium with magnetotactic microorganisms. Appl. Nanosci. 8, 1523–1544 (2018)

[62] Khan, N.S.: Mixed convection in MHD second grade nanofluid flow through a porous medium containing nanoparticles and gyrotactic microorganisms with chemical reaction. Filomat 33, 4627–4653 (2019)

[63] Zuhra, S., Khan, N.S., Shah, Z., Islam, Z., Bonyah, E.: Simulation of bioconvection in the suspension of second grade nanofluid containing nanoparticles and gyrotactic microorganisms. AIP Adv. 8, 105210 (2018)

[64] Zuhra, S., Khan, N.S., Islam, S.: Magnetohydrodynamic second grade nanofluid flow containing nanoparticles and gyrotactic microorganisms. Comput. Appl. Math. 37, 6332–6358 (2018)

[65] Zahra, A., Mahanthesh, B., Basir, M.F.M., Imtiaz, M., Mackolil, J., Khan, N.S., Nabwey, H.A., Tlili, I.: Mixed radiated magneto Casson fluid flow with Arrhenius activation energy and Newtonian heating effects: Flow and sensitivity analysis. Alex. Eng. J. 57, 1019–1031 (2020)

[66] Liaqat, A., Asifa, T., Ali, R., Islam, S., Gul, T., Kumam, P., Mukhtar, S., Khan, N.S., Thounthong, P.: A new analytical approach for the research of thin-film flow of magneto hydrodynamic fluid in the presence of thermal conductivity and variable viscosity. ZAMM J. Appl. Math. Mech. Z. Angewwandte Math. Mech. 101(2), e201900292 (2020)

[67] Khan, N.S., Kumam, P., Thounthong, P.: Second law analysis with effects of Arrhenius activation energy and binary chemical reaction on nanofluid flow. Sci. Rep. 10, 1226 (2020)

[68] Khan, N.S., Shah, Q., Sohail, A.: Dynamics with Cattaneo-Christov heat and mass flux theory of bioconvection Oldroyd-B nanofluid. Adv. Mech. Eng. 12(8), 1–20 (2020)

[69] Shijun, L.: On the homotopy analysis method for non-linear problems. Appl. Math. Comput. 147, 499–513 (2004)

[70] Liaqat, A., Khan, N.S., Ali, R., Islam, S., Kumam, P., Thounthong, P.: Novel insights through the computational techniques in unsteady MHD second grade fluid dynamics with oscillatory boundary conditions. Heat Transf. 50(3), 2502–2524 (2020)

[71] Khan, N.S., Shah, Q., Sohail, A., Kumam, P., Thounthong, P., Bhaumik, A., Ullah, Z.: Lorentz forces effects on the interactions of nanoparticles in emerging mechanisms with innovative approach. Symmetry 12(10), 1700 (2020)

[72] Zuhra, S., Khan, N. S., Islam, S., Nawaz, R.: Complexiton solutions for complex KdV equation by optimal homotopy asymptotic method. Filomat 33(19), 6195–6211 (2020)

[73] Khan, N.S., Ali, L, Ali, R., Kumam, P., Thounthong, P.: A novel algorithm for the computation of systems containing different types of integral and integro-differential equations. Heat Transf. 50(4), 3065–3078 (2020)

[74] Usman, A.H., Khan, N.S., Rano, S.A., Maitama, M., Humphries, U.W.: Study of heat and mass transfer in MHD flow of sutterby ferrofluid over a curved stretching surface with magnetic dipole and chemical reaction effect. Thai J. Math. 19(3), 1037–1055 (2021)

[75] Ramzan, M., Khan, N.S., Kumam, P., Khan, R.: A numerical study of chemical reaction in a nanofluid flow due to rotating disk in the presence of magnetic field. Sci. Rep. 11(1), 19399 (2021)

[76] Ramzan, M., Khan, N.S., Kumam, P.: Mechanical analysis of non-Newtonian nanofluid past a thin needle with dipole effect and entropic characteristics. Sci. Rep. 11(1), 19378 (2021)

[77] Khan, N.S., Humphries, U.W., Kumam, W., Kumam, P., Muhammad, T.: Bioconvection Casson nanoliquid film sprayed on a stretching cylinder in the portfolio of homogeneous-heterogeneous chemical reactions. ZAMM J. Appl. Math. Mech. Z. Angewwandte Math. Mech. 102(5), e202000222 (2022)

[78] Khan, N.S., Humphries, U.W., Kumam, W., Kumam, P., Muhammad, T.: Dynamic pathways for the bioconvection in thermally activated rotating system. Journal of Biomass Conversion and Biorefinery (2022)

[79] Khan, N.S., Humphries, U.W., Kumam, W., Kumam, P., Muhammad, T.: Assessment of irreversibility optimization in Casson nanofluid flow with leading edge accretion or ablation. ZAMM J. Appl. Math. Mech. Z. Angewwandte Math. Mech. 102(10), e202000207 (2022)

[80] Khan, N.S., Fernandez-Gamiz, U., Khan, M.S., Kumam, W., Kumam, P., Galal, A.M.: Thermodynamics of second-grade nanofluid over a stretchable rotating porous disk subject to Hall current and cubic autocatalysis chemical reactions. Front. Phys. 10, 961774 (2022)

[81] Khan, N.S., Sriyab, S., Kaewkhao, A., Thawinan, E.: Hall current effect in bioconvection Oldroyd-B nanofluid flow through a porous medium with Cattaneo-Christov heat and mass flux theory. Sci. Rep. 12, 19821 (2022)

How to cite this article: Khan, N.S., Hussanan, A., Kumam, W., Kumam, P., Suttiarporn, P.: Accessing the thermodynamics of Walter-B fluid with magnetic dipole effect past a curved stretching surface. Z Angew Math Mech. 103, e202100112 (2023). https://doi.org/10.1002/zamm.202100112